Frontiers in Bioscience Landmark

Front. Biosci. (Landmark Ed) **2025**; 30(6): 37052
https://doi.org/10.31083/FBL37052

Original Research

TRPV1 Inhibits Ferroptosis and Mitophagy to Alleviate Heart Failure by Activating *SFXN2*

Pan Liu[1], Shiguang Wang[2], Liya Li[1], Ruihua Li[1], Minming Fan[1], Jingjing Kong[1], Bing Gao[3], Jing Wang[3,*], Ran Xia[3,*]

[1]Graduate School, Anhui University of Chinese Medicine, Special Project of Xin'an Medical and Traditional Chinese Medicine Modernization Research Institute of Great Health Research Institute, 230012 Hefei, Anhui, China
[2]Department of Cardiology, The First Affiliated Hospital of Anhui University of Chinese Medicine, 230031 Hefei, Anhui, China
[3]Zhongyi School, Anhui University of Chinese Medicine, Special Project of Xin'an Medical and Traditional Chinese Medicine Modernization Research Institute of Great Health Research Institute, 230012 Hefei, Anhui, China
*Correspondence: wangjing2161@126.com (Jing Wang); ranranxia2020@163.com (Ran Xia)
Academic Editor: Natascia Tiso
Submitted: 12 January 2025 Revised: 6 May 2025 Accepted: 27 May 2025 Published: 25 June 2025

Abstract

Background: Heart failure (HF) continues to represent a significant global public health concern. Transient receptor potential cation channel subfamily V member 1 (*TRPV1*) is a calcium-permeable channel that has been linked to cardiac disease and function. However, its significance in HF and underlying processes is unknown. This study aims to determine the regulatory role of *TRPV1* in mitochondrial autophagy in HF. **Methods**: AC16 cardiomyocytes were exposed to angiotensin II (Ang II) to simulate pathological conditions, and changes in oxidative stress were assessed. Transverse aortic constriction (TAC) was used to create a pressure overload-induced HF mouse model, and cardiac-specific *TRPV1* overexpression was achieved by Adeno-associated virus 9 (AAV9). RNA sequencing and bioinformatics analysis were performed to identify *TRPV1*-related mitochondrial genes. Finally, the effects of *TRPV1* overexpression and sideroflexin 2 (*SFXN2*) knockdown on markers related to mitophagy and ferroptosis were analyzed. **Results**: *In vitro*, *TRPV1* overexpression drastically decreased intracellular Ca^{2+} levels, lessened oxidative stress, and reduced Ang II-induced cell death ($p < 0.05$). Bioinformatics analysis identified seven mitochondrial genes associated with *TRPV1*, among which *SFXN2* showed a strong correlation with *TRPV1* ($p < 0.05$). Overexpressing cardiac-specific *TRPV1* in the TAC model led to improved cardiac function, higher fractional shortening and ejection fraction, and reduced levels of mitophagy markers ($p < 0.05$). Mechanistically, *TRPV1* activated *SFXN2*, increasing glutathione peroxidase 4 (*GPX4*) expression and antioxidant capacity (glutathione (GSH), superoxide dismutase (SOD)) while decreasing malondialdehyde (MDA) and ferrous iron (Fe^{2+}) levels ($p < 0.05$). These protective effects were removed by *SFXN2* knockdown. Furthermore, the *TRPV1*-*SFXN2* axis suppressed mitophagy by modulating the PTEN-induced kinase 1 (PINK1)-Parkin-sequestosome 1 (SQSTM1) axis. **Conclusion**: Our results show that *TRPV1* overexpression alleviates Ang II-induced myocardial injury in HF. This protective effect is mediated through *SFXN2*-dependent mitophagy and ferroptosis, highlighting *TRPV1* as a potential therapeutic target for HF.

Keywords: *TRPV1*; heart failure; *SFXN2*; ferroptosis; mitophagy

1. Introduction

Heart failure (HF) is a complicated clinical disease in which abnormal cardiac structure or function leads to impaired ventricular filling or ejection capacity [1]. Patients usually present with symptoms such as exertional dyspnea, paroxysmal nocturnal dyspnea, and orthopnea [2,3]. Valvular heart disease, coronary artery sclerosis, hypertension, and chronic lung diseases such as acute pulmonary infarction and emphysema are potential causes of HF [4]. In addition, physiological stress, such as pregnancy, fatigue, or rapid fluid overload, can increase the burden on the heart and cause myocardial failure in susceptible individuals [5]. The current treatment strategy for HF involves a step-by-step approach. Angiotensin-converting enzyme inhibitors and diuretics are common types of medications used in basic treatment [6]. Beta-blockers, such as metoprolol, are used to treat persistent symptoms by lowering heart rate and cardiac strain [7]. In more severe situations, cardiac resynchronization treatment (CRT) can be used to promote heart contractile coordination. Implantable cardioverter-defibrillator (ICD) treatment is used to prevent sudden death in patients. In addition, the novel Sirtuin 3 (*SIRT3*)-targeted small-molecule agonist 2-amino-4-(3,4-dihydroxyphenyl)-6-hydroxy-pyrimidine-5-carboxamide (2-APOC) has shown potential in the treatment of HF by targeting specific ion channels [8]. This emerging evidence suggests that in-depth research on the regulation of HF-related ion channels in cardiomyocytes may provide important directions for the development of new treatment strategies.

Transient receptor potential cation channel subfamily V member 1 (TRPV1) is an ion channel protein from the

transient receptor potential (TRP) family. Numerous physiological and pathological processes, including pain perception, temperature control, and the inflammatory response, are influenced by *TRPV1*. This molecule has a low permeability to anions but a high permeability to cations such as calcium ions. In recent years, *TRPV1* has become an important target for drug research. Research has shown that aberrant expression of this gene is intimately linked to the development of numerous disorders. As an agonist of TRPV1, capsaicin can not only promote fat decomposition and improve vascular function but also activate *TRPV1* in cardiomyocytes, promote energy metabolism, and reduce myocardial hypertrophy and oxidative stress caused by high salt [9]. On the basis of these important regulatory roles of *TRPV1* in the cardiovascular system, researchers have investigated its therapeutic potential for cardiac remodeling and dysfunction. For example, Horton JS *et al.* [10] reported that *TRPV1* antagonists can be used as a new treatment option for cardiac hypertrophy and HF. *TRPV1*, as a key regulator of the natriuretic peptide signaling pathway, may offer a novel molecular intervention strategy for cardiac hypertrophy and HF. Another rat model study revealed that moxibustion can reduce myocardial damage caused by chronic heart failure (CHF) and normalize cardiac function by regulating the expression of *TRPV1*, thereby reducing myocardial fibrosis [11].

Accumulating data show that ferroptosis is important in the pathophysiology of cardiovascular illnesses. Recent studies have identified key metabolic pathways that regulate ferroptosis, including iron metabolism, glutathione (GSH) metabolism, and lipid metabolism, in various cardiovascular disease models [12,13]. Notably, autophagy, as a key regulator of ferroptosis, regulates cellular iron homeostasis by degrading iron storage proteins such as ferritin, leading to elevated intracellular iron levels and subsequent lipid peroxidation. Mitophagy, a form of selective autophagy, has emerged as a key regulator of HF progression [14]. A member of the sideroflexin (SFXN) protein family, sideroflexin 2 (*SFXN2*), plays a role in the metabolism of iron in the mitochondria. A recent study demonstrated a role for *SFXN2* in regulating heme biosynthesis, with *SFXN2*-knockdown cells showing increased mitochondrial iron content. *SFXN2* overexpression inhibits mitophagy in multiple myeloma cells and increases iron-mediated energy production by inhibiting PTEN-induced kinase 1 (PINK1)/Parkin-mediated mitophagy along with heme oxygenase 1 (HO1)-mediated protection against oxidative stress [15]. However, the role of *SFXN2* in HF is unknown.

HF is a complicated illness with several underlying causes, such as oxidative stress, mitochondrial dysfunction, and cell death. Studies have shown that *TRPV1*, as an ion channel, can regulate calcium homeostasis and inflammatory responses in multiple cell types, but its specific role in HF is not fully understood. This study focused on the regulatory mechanism of *TRPV1* in mitochondrial autophagy and ferroptosis to investigate its role in angiotensin II-induced cardiomyocyte injury and pressure load-induced HF in a mouse model. This analysis of the molecular mechanism of *TRPV1* in HF, especially its role in the *SFXN2*-dependent pathway, provides a new perspective on the possibility of *TRPV1* as a new target for HF therapy.

2. Materials and Methods

2.1 Cell Culture

Human cardiomyocytes AC16 (CL-0790, Procell, Wuhan, Hubei, China) were cultivated in Dulbecco's modified Eagle's medium (DMEM, #G4512-500ML, Servicebio, Wuhan, Hubei, China) supplemented with 10% fetal bovine serum (FBS, #164210; Pricella, Shanghai, China) under standard conditions (37 °C, 5% CO_2). AC16 cells were subjected to short tandem repeat (STR) analysis and Mycoplasma testing. The cells were passaged using 0.25% trypsin (#BL501B; Biosharp, Hefei, Anhui, China) once they reached 70–80% confluence. For cryopreservation, the cells were resuspended in freezing medium consisting of DMEM, FBS, and dimethyl sulfoxide (DMSO, #HY-Y0320C, MCE, Monmouth Junction, NJ, USA) at a ratio of 5:4:1. The cell suspension was transferred into cryovials and gradually cooled to –80 °C overnight before being stored in liquid nitrogen.

2.2 Cell Treatment and Transfection

Angiotensin II (Ang II) is a major regulator of cardiovascular disease, causing cardiomyocyte hypertrophy, fibrosis, and oxidative stress [16]. In this study, AC16 human cardiomyocytes were treated with 1 µmol/L Ang II (#HY-13948, MCE, Monmouth Junction, NJ, USA) for 24 hours to establish a cell model that mimics the pathological conditions of HF. The small interfering RNA (siRNA) sequences targeting *SFXN2* (**Supplementary Material 1**), the *TRPV1* overexpression plasmid (**Supplementary Material 2**) and the negative control (OE-NC, pRP[Exp]-CMV>ORF_Stuffer) were synthesized by General Biotechnology Co., Ltd. (Hefei, Anhui, China) and Vectorbuilder (Guangzhou, Guangdong, China). For *TRPV1* overexpression, AC16 cells were added to 6-well plates to 70% confluency and transfected with the *TRPV1* overexpression plasmid using Lipo8000™ transfection reagent (#C0533; Beyotime, Shanghai, China) according to the manufacturer's instructions. Transfection complexes were prepared by mixing plasmid DNA with Lipo8000™ reagent in serum-free medium and incubating for 10–15 minutes. For *SFXN2* knockdown, cells were transfected with 2.5 µL of siRNA targeting *SFXN2* (Si-*SFXN2*) or a negative control (Si-NC) using the same method. For the cotransfection experiments, the *TRPV1* plasmid and Si-*SFXN2* (or Si-NC) were co-delivered into the cells after 6 h, and the medium was changed to com-

plete medium supplemented with 10% FBS. The cells were cultured for 24 hours before further analysis.

2.3 Animals

Eight- to twelve-week-old C57BL/6J male mice (20–25 g) (total = 32) were obtained from Liaoning Changsheng Biotechnology Co., Ltd. (Shenyang, Liaoning, China), which maintains specific pathogen-free certification (SCXK[Liao]2020–000). Every animal experiment was carried out in compliance with the rules and regulations that were authorized by the Animal Ethics Committee's Institutional Animal Care and Use Committee of The First Affiliated Hospital of Anhui University of Chinese Medicine (AZYFY-2024-1006). All experiments were conducted in accordance with the 3R principles. Research was conducted at the Anhui Provincial Key Laboratory of Meridians and Organs. The animals were maintained at 22 ± 2 °C under controlled lighting (12 h cycles) with unrestricted access to standard chow and water.

2.4 Transverse Aortic Constriction (TAC) and Adeno-Associated Virus 9 (AAV9) Injection

The mice were randomly assigned to four groups: the sham, TAC, TAC+AAV9-cardiac troponin T (CTNT)-control, and TAC+AAV9-CTNT-*TRPV1* groups (n = 8 per group). The mice were anesthetized with ketamine (100 mg/kg) and xylazine (10 mg/kg) (6–1712, Bingene, Beijing, China) via intraperitoneal injection. TAC surgery was conducted as previously described [17] to create a mouse model of cardiac hypertrophy and HF. Sham-operated control mice underwent the same surgery but without aortic constriction. AAV9 was used to achieve cardiac-specific overexpression of *TRPV1*. The AAV9-*TRPV1* vector was constructed by inserting mouse *TRPV1* complementary DNA (cDNA) under the control of the promoter (**Supplementary Material 3**). The AAV9-CTNT-control vector (AAV00274Z, Creative-Biogene, Shirley, NY, USA) without any exogenous gene was used as a control. AAV9 vectors (1×10^{11} viral genome particles per mouse) were administered by tail vein injection. After 2 weeks, the infected mice were subjected to TAC for 28 days. After the study, euthanasia was performed using an overdose of sodium pentobarbital (150 mg/kg, intraperitoneal injection).

2.5 Echocardiographic Analysis

Cardiac function was evaluated using a Vevo 2100 system (VisualSonics, Toronto, ON, Canada) with a 30 MHz transducer at week 8 post-surgery. Under 2% isoflurane (#R510-22-10, RWD, Shenzhen, Guangdong, China) anesthesia and temperature monitoring, parasternal short-axis M-mode images were acquired at the papillary muscle level. Left ventricular (LV) functional parameters, including the ejection fraction (EF) and fractional shortening (FS), were analyzed via Vevo Lab software (version 3.1.1, FUJIFILM VisualSonics Inc., Toronto, ON, Canada) by an independent operator unaware of group allocation. All echocardiographic measurements were carried out by an experienced operator who was unaware of the experimental groups.

2.6 RNA Isolation and Sequencing

Following the manufacturer's instructions, TRIzol reagent (#G3013-100ML; Life Technologies, Carlsbad, CA, USA) was used to separate total RNA from AC16 cells. The RNA concentration and purity were evaluated via an OD1000+ ultramicrospectrophotometer (Nanjing Wuyi Technology Co., Ltd., Nanjing, Jiangsu, China). Samples showing intact RNA bands on 1% agarose gels (ST004L, Beyotime, Shanghai, China) and RNA integrity number (RIN) values exceeding 8 qualified for library construction. The NEBNext Ultra RNA Library Prep Kit for Illumina (#E7530L; New England Biolabs, Ipswich, MA, USA) was used to produce RNA sequencing (RNA-seq) libraries in accordance with the manufacturer's instructions. Poly-T magnetic beads were used to isolate mRNA for fragmentation. Double-stranded cDNA was generated through reverse transcription with random hexamers followed by second-strand synthesis. After that, the double-stranded cDNA underwent PCR amplification, adapter ligation, end repair, and A-tailing. A Qubit 2.0 fluorometer (Thermo Fisher Scientific, Waltham, MA, USA) was used to quantify the final cDNA libraries, and an Agilent 2100 Bioanalyzer (Agilent Technologies, Inc., Santa Clara, CA, USA) was used for validation. The libraries were sequenced using 150 bp paired-end reads on an Illumina NovaSeq 6000 platform (Illumina, San Diego, CA, USA). Shanghai OE Biotech. Co., Ltd. (Shanghai, China) carried out the RNA sequencing. For every group, three biological replicates were conducted.

2.7 Bioinformatic Analysis

The "limma" package (version 3.54.0) in R (version 4.0.3, R Foundation for Statistical Computing, Vienna, Austria) was used to perform differential gene expression analysis between the control and *TRPV1* overexpression groups. Genes with $|\log_2\text{-fold change (FC)}| \geq 1$ and $p < 0.05$ were considered differentially expressed genes (DEGs). Gene Ontology (GO) and Kyoto Encyclopedia of Genes and Genomes (KEGG) pathway enrichment analyses were performed using the Database for Annotation, Visualization, and Integrated Discovery (DAVID; https://david.ncifcrf.gov/). Both the GO and KEGG pathway enrichment results were deemed statistically significant when the p value was less than 0.05.

2.8 Identification of TRPV1-Associated Mitochondria-Related Genes (Mito-RGs)

A total of 1576 Mito-RGs were collected from the Molecular Signature Database (MSigDB, https://www.gs

Table 1. List of antibodies used for Western blot analysis.

Antibody	Cell (Dilution; Item No.; Manufacturer)	Tissue (Cell (Dilution; Item No.; Manufacturer))
Transient receptor potential cation channel subfamily V member 1 (TRPV1)	1:500, #DF10320, Affinity Biosciences, Liyang, Jiangsu, China	1:1000, #DF10320, Affinity Biosciences, Liyang, Jiangsu, China
Sideroflexin 2 (SFXN2)	1:1000, #BS77506, Bioworld Technology, Chongqing, China	1:1000, #BS77506, Bioworld Technology, Chongqing, China
Glutathione peroxidase 4 (GPX4)	1:500, #DF6701, Affinity Biosciences, Liyang, Jiangsu, China	1:1000, #DF6701, Affinity Biosciences, Liyang, Jiangsu, China
Parkin	1:500, #AF0235, Affinity Biosciences, Liyang, Jiangsu, China	1:500, #2132, Cell Signaling Technology, Danvers, MA, USA
PTEN-induced kinase 1 (PINK1)	1:1000, #DF7742, Affinity Biosciences, Liyang, Jiangsu, China	1:1000, #DF7742, Affinity Biosciences, Liyang, Jiangsu, China
Sequestosome 1 (SQSTM1)	1:5000, #66184-1-Ig, Proteintech, Wuhan, Hubei, China	1:5000, #66184-1-Ig, Proteintech, Wuhan, Hubei, China
Atrial natriuretic peptide (ANP)	/	1:500, #DF6497, Affinity Biosciences, Liyang, Jiangsu, China
Beta-myosin heavy chain (β-MHC)	/	1:500, #ab23990, Abcam, Cambridge, Cambridgeshire, UK
Glyceraldehyde-3-phosphate dehydrogenase (GAPDH)	1:5000, #380626, ZENBIO, Chengdu, Sichuan, China	1:5000, #380626, ZENBIO, Chengdu, Sichuan, China
Voltage-dependent anion channel 1 (VDAC1)	1:500, #AF5478, Affinity Biosciences, Liyang, Jiangsu, China	1:500, #AF5478, Affinity Biosciences, Liyang, Jiangsu, China

ea-msigdb.org/gsea/msigdb/). The overlapping genes between 249 *TRPV1*-related genes and 1576 Mito-RGs were identified using the Venn online graphical tool (https://bioinformatics.psb.ugent.be/webtools/Venn/).

2.9 Correlation Analysis Between TRPV1 and Mito-RG Expression

The sequencing datasets (containing the control group and the *TRPV1* overexpression group) were used to assess the expression levels of seven overlapping genes. The raw counts were normalized with DESeq2 (version 1.30.1) in R, and the $\log_2$-transformed normalized expression values were visualized with pheatmap (version 1.0.12). The correlation matrix of the seven genes was calculated and visualized using a corrplot (version 0.84). The Spearman correlation coefficient between *TRPV1* and each of the seven Mito-RGs was calculated in R using the Spearman method. Scatter plots with trend lines were generated using ggplot2 (version 3.3.3) to visualize the correlations.

2.10 Subcellular Fractionation

Mitochondria and the cytosol were isolated from cardiac tissue via a Tissue Mitochondria Isolation Kit (#C3606, Beyotime, Shanghai, China) and a Tissue Cytoplasm and Nucleus Separation Kit (#NT-032, Invent, Wilmington, DE, USA) according to the manufacturer's instructions. Similarly, mitochondria and cytosol from AC16 cells were extracted using the Cell Mitochondria Isolation Kit (#C3601, Beyotime, Shanghai, China) and the Cell Cytoplasm and Nucleus Separation Kit (#BB-36021, Beibokit, Shanghai, China) following the manufacturer's protocols.

2.11 Western Blot Analysis

Proteins in cardiac tissue and AC16 cells (mitochondria) were extracted with radioimmunoprecipitation assay (RIPA) buffer (#P0013, Beyotime, Shanghai, China). After the samples were homogenized, they were incubated on ice for 30 minutes and then centrifuged at 12,000 $\times$g for 15 minutes (4 °C). The supernatant was then collected. Protein quantification was performed with a bicinchoninic acid (BCA) kit (P0012, Beyotime, Shanghai, China). The samples (30 µg) were denatured in loading buffer (100 °C, 10 min) and resolved by 10% sodium dodecyl sulfate–polyacrylamide gel electrophoresis (SDS–PAGE) (#P0690, Beyotime, Shanghai, China) (stacking: 80 V; separating: 120 V). Proteins were electroblotted onto methanol-activated polyvinylidene fluoride (PVDF) (#FFP24, Beyotime, Shanghai, China) membranes (300 mA, 90 min). After being blocked with 5% milk-Tris-buffered saline with Tween 20 (TBST) (60145ES76, YEASEN, Shanghai, China) (2 h), the membranes were probed with primary antibodies (Table 1) overnight at 4 °C, followed by incubation with HRP-conjugated secondary antibodies (goat anti-mouse IgG (ZB-2305, Zs-BIO, Beijing, China), goat anti-rabbit IgG (ZB-2301), Zs-BIO, Beijing, China) (1:10,000, 1 h). The membrane was exposed to enhanced chemiluminescence detection reagent (KGC4902, Keygene, Nan-

Table 2. Primer sequences and amplicon sizes used for quantitative real-time polymerase chain reaction (qRT–PCR) analysis.

Gene	Size (bp)	Forward primer (5′-3′)	Reverse primer (5′-3′)
Hu-*TRPV1*	195	CCACTCTTCTCCCACACGAG	GGCAGGTGTCCTTTTGGAGT
G0/G1 switch gene 2 (*G0S2*)	118	TCCACCAAAGGAGTTTGGGA	TCCTTCCTCCCTAGTGCAAA
Solute Carrier Family 25 Member 24 (*SLC25A24*)	121	TATCCAGCACCTGTGGTCAG	ATTCGTCGAAAGAGGCCAAC
Schindler Disease (*SDS*)	194	CCCATCCTTAGCCACCTTGC	GGATGGCTGAGATGGTTCCT
Sideroflexin 2 (*SFXN2*)	120	AAGGGAATCTGCGTGAAGGA	GATCATCCCAGGAGCTGACA
Creatine Kinase Mitochondrial 2 (*CKMT2*)	192	AAAGATCACCCAAGGGCAGT	TCGGACAGCTTGTAGTAGCG
Tubulin Polymerization Promoting Protein (*TPPP*)	113	CCTTCTCCACTCAGCTCCAA	GGTGACCACTATGTCCTCGT
GAPDH	138	CGGATTTGGTCGTATTGG	GGTGGAATCATATTGGAACA

jing, Jiangsu, China), and gel imaging was performed using gel imaging equipment (Bio-Rad, Hercules, CA, USA) for protein visualization. The grayscale density of the protein bands was quantified using ImageJ software (version 1.8.0; National Institutes of Health, Bethesda, MD, USA). Glyceraldehyde-3-phosphate dehydrogenase (GAPDH) and voltage-dependent anion channel 1 (VDAC1) were used as cytosolic and mitochondrial markers, respectively.

2.12 Quantitative Real-Time Polymerase Chain Reaction (qRT–PCR)

TRIzol reagent (#G3013-100ML; Life Technologies, Carlsbad, CA, USA) was used to extract total RNA from AC16 cardiomyocytes. An OD1000+ ultramicrospectrophotometer (Nanjing Wuyi Technology Co., Ltd., Nanjing, Jiangsu, China) was used to measure the concentration and purity of the RNA, and 1% agarose gel electrophoresis was used to confirm the integrity of the RNA. With a reverse transcription kit with dsDNAse (#BL699A; Biosharp, Hefei, Anhui, China) and a PTC-200 heat cycler (Bio-Rad, Hercules, CA, USA), first-strand cDNA was generated. The reaction proceeded for 30 min at 37 °C followed by 5 min at 85 °C. qRT–PCR was carried out with an ABI StepOne Plus Real-Time PCR System with Taq SYBR Green qPCR Premix Universal (#EG20117M, Bestenzymes, Lianyungang, Jiangsu, China). A 20 µL PCR mixture was prepared with SYBR Green premix (10 µL), primers (0.4 µL each, 10 µM, Sangon Biotech, Shanghai, China), cDNA (3 µL), and Diethylpyrocarbonate-treated Water (DEPC-H_2O) (6.2 µL, #D1007; Generay Biotech, Shanghai, China). Initial denaturation at 95 °C for 30 s was followed by 40 cycles of 95 °C for 15 s and 60 °C for 30 s as part of the amplification process. Melting curve analysis was used to establish the specificity of amplification. The expression levels of *TRPV1* and mitochondria-related genes were analyzed. The internal reference gene was *GAPDH*. Table 2 lists the specific sequences of the primers used. The relative expression of genes was calculated using the $2^{-\Delta\Delta CT}$ method.

2.13 Determination of Oxidative Stress and Ferroptosis Markers

A bicinchoninic acid (BCA) protein assay kit (#BL521A; Biosharp, Hefei, Anhui, China) was used to measure the protein concentration of the homogenate after AC16 cells from various treatment groups were obtained and homogenized in ice-cold phosphate-buffered saline (PBS, #G4207; Servicebio, Wuhan, Hubei, China). The malondialdehyde (MDA), superoxide dismutase (SOD), glutathione (GSH), and ferrous iron (Fe^{2+}) levels associated with lipid peroxidation were subsequently measured using an MDA assay kit (#A003-1-2), a SOD kit (#A001-3-1), a reduced GSH assay kit (#A006-2-1), and a ferrous ion colorimetric kit (#E-BC-K773-M; Elabscience, Wuhan, Hubei, China). All unlabeled kits were provided by Nanjing Jiancheng Bioengineering Institute (Nanjing, Jiangsu, China). Every test was carried out in compliance with the manufacturer's instructions. The absorbance was measured at 532 nm (MDA), 450 nm (SOD), 420 nm (GSH), and 593 nm (Fe^{2+}) using a microplate reader (Bio-Rad, Hercules, CA, USA). The quantitative methods were performed according to the instructions provided in the manual.

2.14 Measurement of the Intracellular Calcium Concentration (Ca^{2+})

The intracellular Ca^{2+} concentration of AC16 cells was analyzed using a calcium assay kit (#40776ES50, YEASEN, Shanghai, China) according to the manufacturer's instructions. In brief, AC16 cells were extracted via centrifugation at 1000 rpm for 5 minutes and then rinsed with PBS. The cells were then incubated with 5 µM Rhod-2 AM (prepared in DMSO with a 2–5 mM stock solution) for 30 minutes at 37 °C in the dark. The cells were washed twice with PBS, followed by centrifugation (1000 rpm, 5 min). Fluorescence images were captured with a Leica DMI3000B inverted fluorescence microscope (Leica, Wetzlar, Hesse, Germany) at 200× magnification. Calcium-bound Rhod-2 AM fluorescence was detected using an appropriate red fluorescence filter, and the green fluorescent protein (GFP) signal was monitored in the green channel. Quantification was performed using ImageJ software.

2.15 Calcein Acetoxymethyl Ester (Calcein AM)/Propidium Iodide (PI) Staining

Following the manufacturer's instructions, cell viability was evaluated using the Calcein AM/PI Live/Dead Viability/Cytotoxicity Assay Kit (#C2015M; Beyotime, Shanghai, China). After being washed with PBS, AC16 cells from various treatment groups were treated with the working solution for 30 minutes at 37 °C in the dark. PI (red fluorescence) was used to identify dead cells, whereas Calcein AM (green fluorescence) was used to identify live cells. Fluorescence images were taken at 200× magnification using an Olympus CKX53 inverted microscope (Olympus, Tokyo, Japan), and at least three random fields of view were taken for each group. Images were acquired using appropriate filter sets for the PI (red) and Calcein AM (green) channels and then merged for analysis. Cell viability was quantified using ImageJ software.

2.16 Mitochondrial Reactive Oxygen Species (ROS) Detection

MitoSOX Red (HY-D1055, MCE, Monmouth Junction, NJ, USA) was used to assess the levels of ROS in the mitochondria. AC16 cells were plated, rinsed with PBS, and then incubated with 5 µM MitoSOX Red working solution at 37 °C for 30 minutes in the dark. Nuclei were counterstained with 4′,6-diamidino-2′-phenylindole (DAPI, #C1002; Beyotime, Shanghai, China). Fluorescence images were captured at 200× magnification using a Leica DMI3000B inverted fluorescence microscope. At least three random fields were taken for each group. Red fluorescence indicates mitochondrial superoxide levels, while DAPI staining (blue) was used for nuclear visualization. The ROS level was quantified using ImageJ software.

2.17 Terminal Deoxynucleotidyl Transferase dUTP Nick-End Labeling (TUNEL) Assay

Apoptotic cells were detected via a one-step TUNEL kit (#ECK-A320; Elabscience, Wuhan, Hubei, China). The samples were fixed in 4% paraformaldehyde (CF189021, Solarbio, Beijing, China) (30 min) and permeabilized with 0.2% Triton X-100 (P0096, Beyotime, Shanghai, China) (5 min) in PBS. After washing, the samples were incubated in the dark (37 °C, 1 h) with a TdT/luciferin-dutP reaction mixture. Nuclear staining was performed with DAPI (25 µg/mL, 10 min). Images were acquired at 100× magnification, and TUNEL-positive cells (green) were quantified relative to total DAPI signals (blue) using ImageJ software.

2.18 Statistical Analysis

Data analysis was performed with R (version 4.0.3, R Foundation for Statistical Computing, Vienna, Austria) and GraphPad Prism (version 8.0.0, GraphPad Software, San Diego, CA, USA). The results represent the mean ± standard deviation (standard deviation) from three independent experiments. Differences between pairs were evaluated by Student's *t*-test, whereas multigroup analyses employed one-way analysis of variance (ANOVA) with Tukey's post hoc comparisons. Statistical significance was set at $p < 0.05$.

3. Results

3.1 TRPV1 Overexpression Reduces Intracellular Ca^{2+} Levels in AC16 Cardiomyocytes

AC16 human cardiomyocytes were treated with 1 µmol/L Ang II to simulate pathological cardiac conditions. *TRPV1* mRNA expression was significantly downregulated according to qRT–PCR ($p < 0.0001$, Fig. 1A). Western blot analysis revealed that *TRPV1* protein levels were similarly reduced following Ang II stimulation ($p < 0.001$, Fig. 1B). To investigate the effect of *TRPV1*, we first overexpressed *TRPV1* in AC16 cells ($p < 0.0001$, Fig. 1C,D). Next, the intracellular Ca^{2+} level in AC16 cells was assessed using fluorescent probes. Compared with that in the control group, *TRPV1* overexpression significantly reduced the intracellular Ca^{2+} level ($p < 0.05$, Fig. 2A). OE-TRPV1 increased the level of TRPV1 in the HF cell model, which was validated via qRT–PCR and Western blot analyses ($p < 0.0001$, Fig. 2B,C).

3.2 TRPV1 Alleviates Ang II-Induced Cell Death and Oxidative Stress

To investigate whether *TRPV1* affects cell viability under Ang II stimulation, we performed PI/Calcein AM double staining. Compared with the control treatment, Ang II treatment dramatically inhibited cell viability ($p < 0.001$, **Supplementary Fig. 1**). Overexpression of *TRPV1* reversed the Ang II-induced decrease in cell viability ($p < 0.05$, **Supplementary Fig. 1**). Next, the intracellular ROS levels were examined using fluorescence imaging. A comparison of the Ang II-treated group with the control group revealed a substantial increase in ROS generation ($p < 0.0001$, **Supplementary Fig. 2**). Notably, overexpression of *TRPV1* significantly attenuated the increase in ROS levels induced by Ang II ($p < 0.001$, **Supplementary Fig. 2**). These results suggest that by preventing oxidative stress, *TRPV1* overexpression shields cardiomyocytes from Ang II-induced harm.

3.3 Identification and Enrichment Analysis of TRPV1-Related Differentially Expressed Genes

According to the screening criteria for DEGs, 195 upregulated genes and 54 downregulated genes were screened from the sequencing data (**Supplementary Fig. 3**). The results of the biological process (BP), cellular component (CC), and molecular function (MF) enrichment analyses revealed that the upregulated genes were associated primarily with nucleosomes (GO: 0000786), the deoxyribonucleic acid (DNA) packaging complex (GO: 0044815), protein heterodimerization activity (GO: 0046982), DNA binding

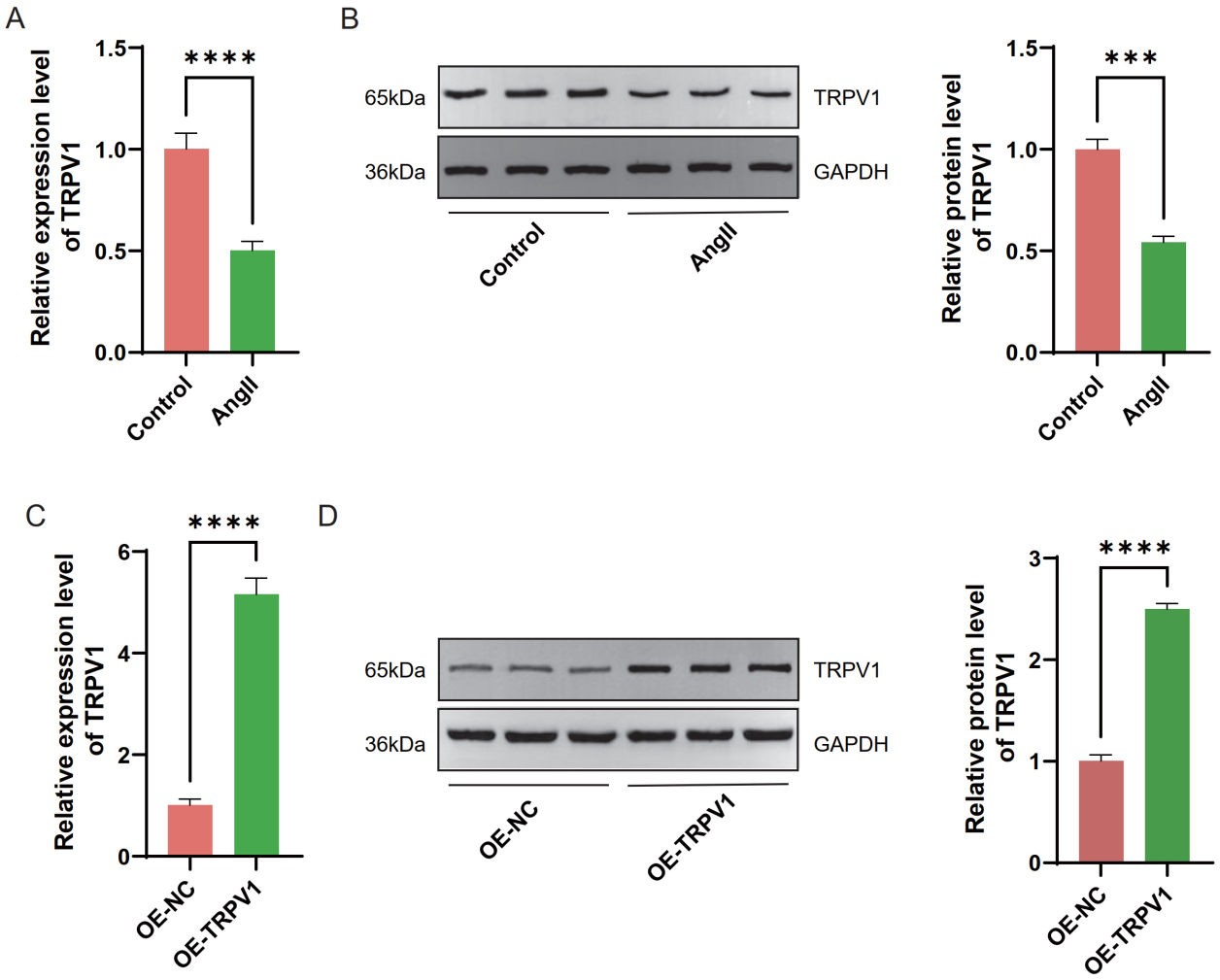

Fig. 1. Analysis of transient receptor potential cation channel subfamily V member 1 (*TRPV1*) level in AC16 cells induced by angiotensin II (Ang II) and overexpressing TRPV1. (A) Quantitative real-time polymerase chain reaction (qRT–PCR) detected the *TRPV1* mRNA level in AC16 cells induced by Ang II. (B) Western blot analysis of TRPV1 protein levels in AC16 cells after Ang II induction was performed and glyceraldehyde-3-phosphate dehydrogenase (GAPDH) was used for normalization. (C) qRT–PCR detected the *TRPV1* mRNA level of AC16 cells in overexpression negative control (OE-NC) and overexpression *TRPV1* (OE-*TRPV1*) groups. (D) Western blot analysis of TRPV1 protein levels of AC16 cells in OE-NC and OE-TRPV1 groups was performed, and GAPDH was used for normalization. Each experiment was independently repeated three times. Data are presented as mean ± standard deviation. ***$p < 0.001$, ****$p < 0.0001$.

(GO: 0003677), and nucleosome assembly (GO: 0006334) (**Supplementary Fig. 4A**). The downregulated genes were related to the extracellular region (GO: 0005576), cytokine activity (GO: 0005125), cell adhesion (GO: 0007155), and the cell surface receptor signaling pathway (GO: 0007166) (**Supplementary Fig. 4B**). KEGG enrichment pathway analysis revealed that the pathways enriched with the upregulated genes included the apelin signaling pathway, herpes simplex virus 1 infection, and alcoholism (**Supplementary Fig. 5A**). The downregulated genes were associated with KEGG pathways such as the chemokine signaling pathway, NOD-like receptor signaling pathway, influenza A pathway, and the interleukin-17 (IL-17) signaling pathway (**Supplementary Fig. 5B**).

3.4 Identification of TRPV1-Mitochondrial Gene Interactions

To explore the possible molecular mechanisms underlying the relationship between *TRPV1* and mitochondrial function, we performed an intersection analysis of *TRPV1*-related genes and Mito-RGs. Venn diagram analysis revealed that there were 7 overlapping genes between the *TRPV1*-related genes (249 genes) and Mito-RGs (1576 genes) (Fig. 3A). Among these overlapping genes, heatmap analysis revealed different expression patterns between the groups (Fig. 3B). Further analysis revealed differences in correlations between different genes (Fig. 3C). For example, solute carrier family 25 member 24 (*SLC25A24*) and G0/G1 switch gene 2 (*G0S2*) were strongly positively cor-

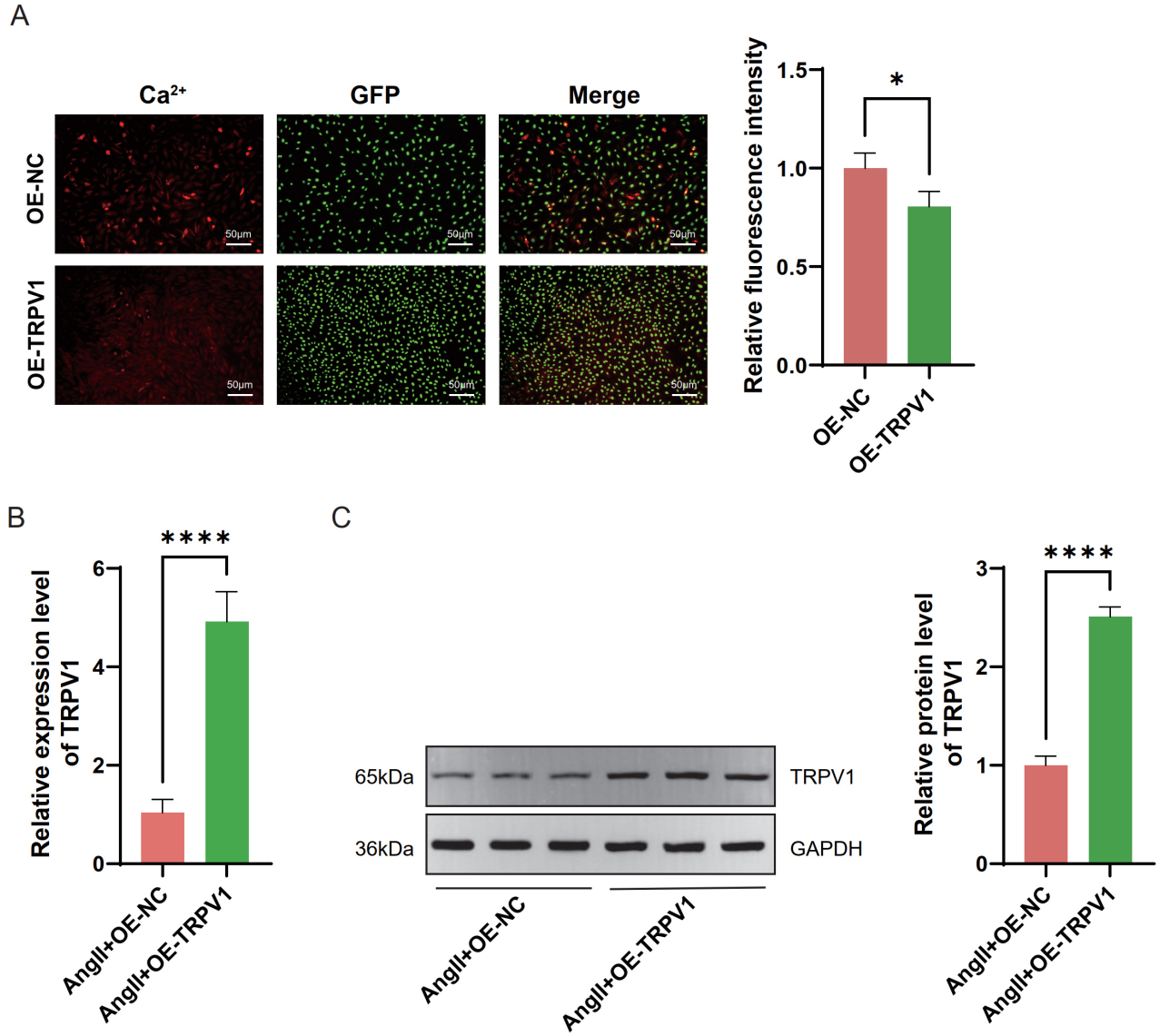

Fig. 2. Effects of *TRPV1* overexpression on intracellular Ca^{2+} levels and TRPV1 expression in heart failure (HF) cell model. (A) Representative fluorescence microscopy images showing intracellular calcium ion (Ca^{2+}) levels (red), green fluorescent protein (GFP) expression (green), and merged images in OE-NC and OE-*TRPV1* groups. Magnification: 200×. Scale bar = 50 μm. (B) qRT–PCR was used to detect the *TRPV1* mRNA level in HF cell model transfected with OE-TRPV1. (C) Western blot detection of TRPV1 protein level in HF cell model transfected with OE-TRPV1, and GAPDH was used for normalization. Each experiment was independently repeated three times. Data are presented as mean ± standard deviation. *$p < 0.05$, ****$p < 0.0001$.

related, whereas *SLC25A24* was significantly negatively correlated with tubulin polymerization promoting protein (*TPPP*) and lactate dehydrogenase A like 6B (*LDHAL6B*) ($p < 0.01$, Fig. 3C). These findings suggest that there is a complex regulatory network between *TRPV1* and Mito-RGs, which may contribute to the role of *TRPV1* in mitochondrial function.

3.5 Correlation Analysis of TRPV1 and TRPV1-Mito DEGs and Their Expression in HF

Further analysis confirmed the correlation between *TRPV1* and seven genes (**Supplementary Fig. 6A–G**). Strong correlations were observed between *TRPV1* and both *LDHAL6B* ($p = 0.03$, r = 0.86) and *SFXN2* ($p = 0.04$, r = 0.83) (**Supplementary Fig. 6C,E**). *In vitro* experiments verified the expression of these genes in AC16 cells treated with Ang II. After *TRPV1* overexpression, qRT–PCR analysis revealed that the expression of schindler disease (*SDS*), *SFXN2*, creatine kinase mitochondrial 2 (*CKMT2*), *TPPP*, and *LDHAL6B* was dramatically greater than that in the Ang II+OE-NC group ($p < 0.001$), whereas the *G0S2* and *SLC25A24* levels were not significantly altered (**Supplementary Fig. 6H**). Among these genes, *LDHAL6B* and *SFXN2* presented the strongest correlations

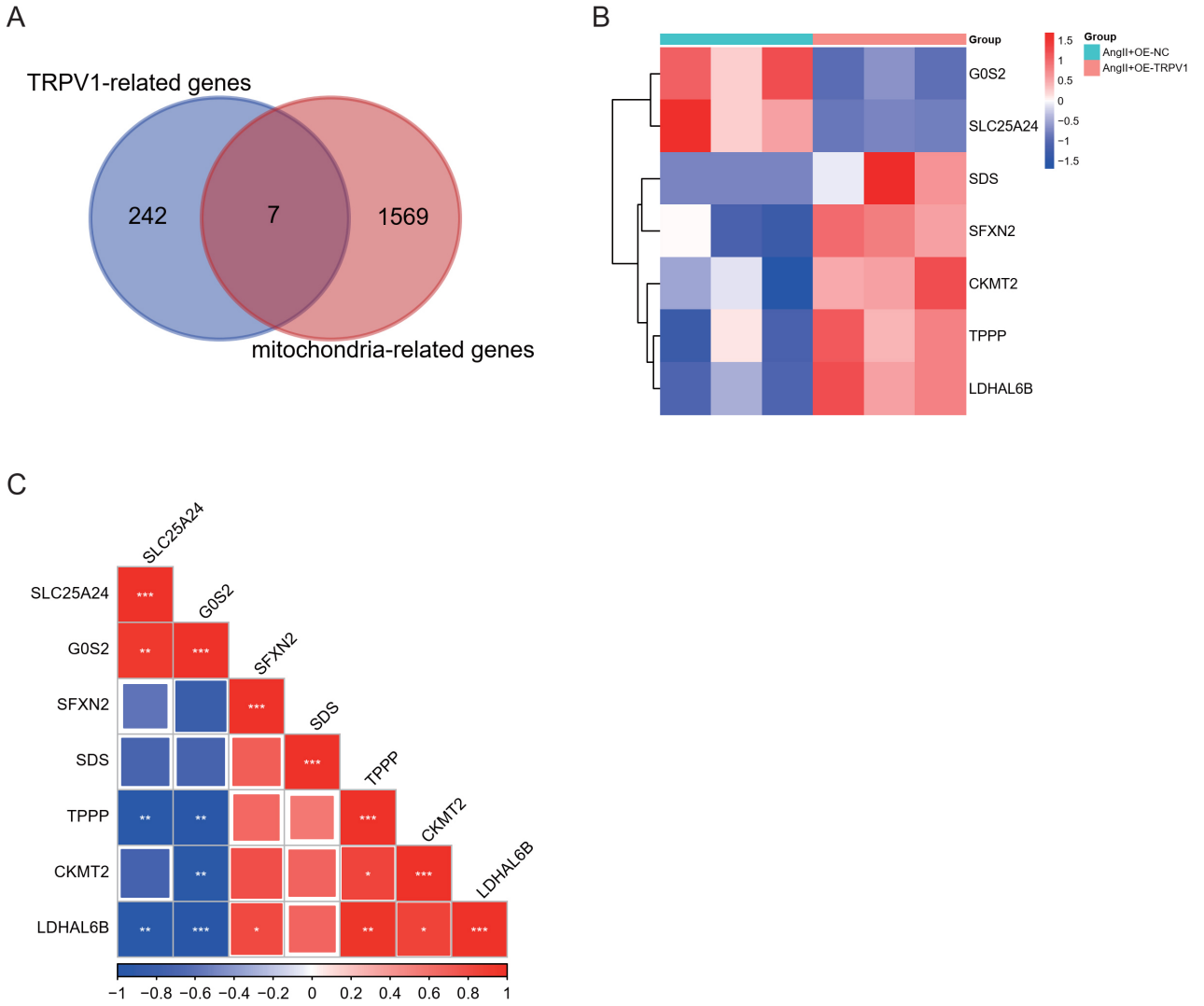

Fig. 3. Analysis of *TRPV1* and mitochondria-related gene expression patterns. (A) Venn diagram showing the overlap between *TRPV1*-related genes and mitochondria-related genes. (B) Heatmap visualization of expression patterns for the seven overlapping genes across different experimental groups. Color scale represents normalized expression values, with red indicating upregulation and blue indicating downregulation. (C) Correlation matrix showing the relationships among the seven overlapping genes. The size and color intensity of squares represent correlation strength (–1 to 1), with blue indicating negative correlations and red indicating positive correlations. Statistical significance is denoted by asterisks (*$p < 0.05$, **$p < 0.01$, ***$p < 0.001$). LDHAL6B, lactate dehydrogenase A like 6B.

with *TRPV1*. The role of *SFXN2* in mitochondrial function has been previously established. However, its specific involvement in mitochondrial function during HF remains unclear. Therefore, we selected *SFXN2* for further analysis.

3.6 TRPV1-Targeted Therapy Alleviates TAC-Induced HF

To assess the therapeutic potential of *TRPV1* in HF, we generated a model of cardiac dysfunction caused by pressure overload using TAC. Cardiac function was assessed using echocardiography. Compared with those in the sham group, the cardiac function of the mice in the TAC-treated group was considerably worse, as evidenced by a reduction in FS and EF ($p < 0.0001$, **Supplementary Fig. 7A–C**). Notably, compared with TAC+AAV9-CTNT-control, AAV9-mediated cardiac-specific *TRPV1* overexpression (TAC+AAV9-CTNT-*TRPV1*) improved cardiac function, as shown by a moderate increase in EF and FS ($p < 0.0001$, **Supplementary Fig. 7A–C**). Compared with those in the sham group, TAC dramatically decreased the expression of *TRPV1* and *SFXN2* while increasing the protein levels of atrial natriuretic peptide (ANP) and beta-myosin heavy chain (β-MHC) ($p < 0.0001$, Fig. 4A–E). Moreover, compared with those in the TAC+AAV9-CTNT-control group, *TRPV1* overexpression significantly increased TRPV1 and SFXN2 protein levels but significantly reduced the expression of the cardiac stress markers ANP and β-MHC ($p <$

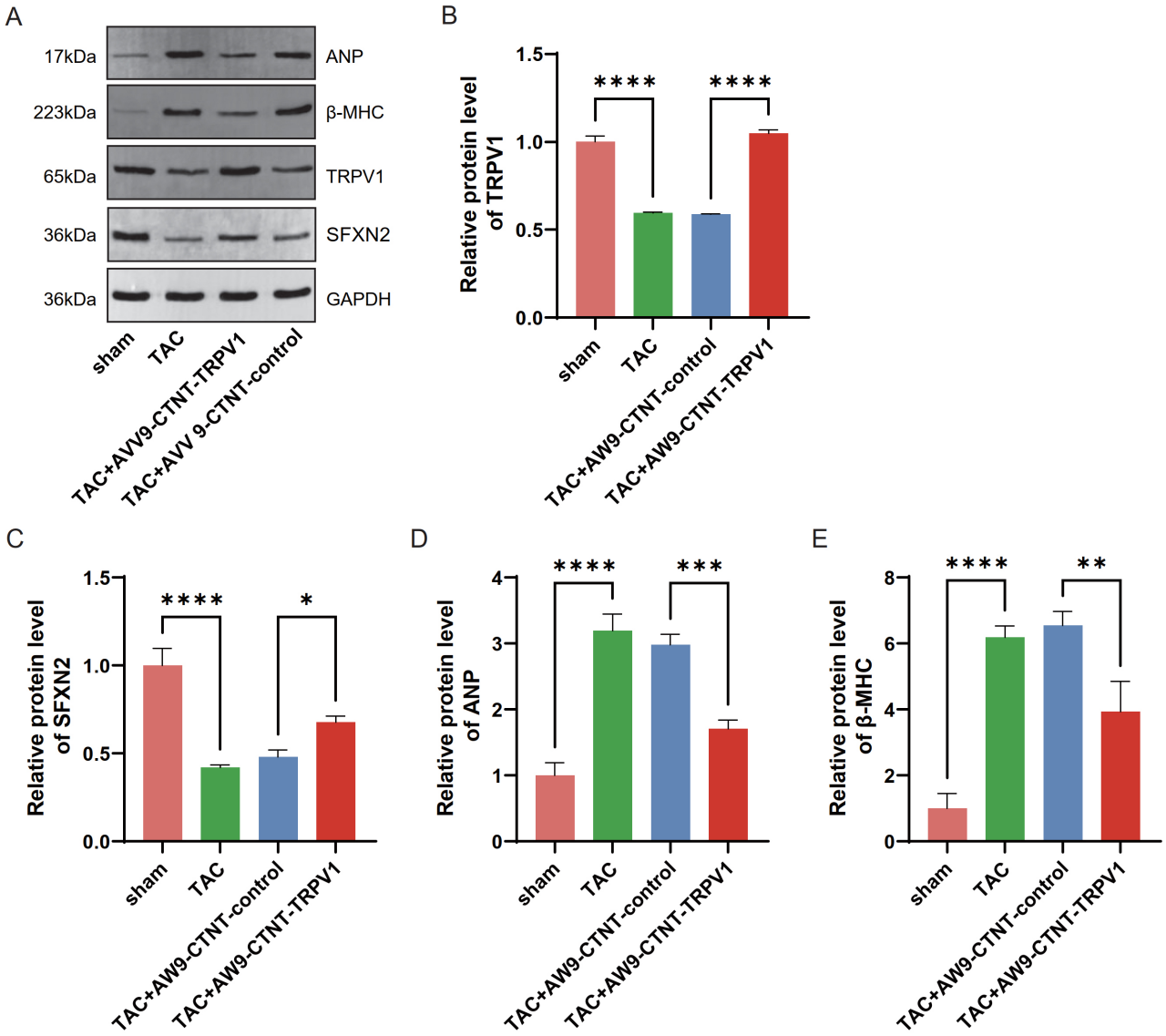

Fig. 4. *TRPV1* overexpression regulates the expression of HF-related markers in the TAC-induced HF model. (A) Representative Western blot images showing protein expression of HF-related markers (atrial natriuretic peptide (ANP), beta-myosin heavy chain (β-MHC), TRPV1, and sideroflexin 2 (SFXN2)) in different experimental groups (sham, transverse aortic constriction (TAC), TAC+adeno-associated virus 9 (AVV9)-cardiac troponin T (CTNT)-control, TAC+AVV9-CTNT-*TRPV1*), with GAPDH as a loading control. (B–E) Quantitative analysis of protein expression levels of TRPV1 (B), SFXN2 (C), ANP (D), and β-MHC (E) with GAPDH as a standard. Each experiment was independently repeated three times. Data are presented as mean $\pm$ standard deviation. *$p < 0.05$, **$p < 0.01$, ***$p < 0.001$, ****$p < 0.0001$.

0.05, Fig. 4A–E). These results suggest that *TRPV1* overexpression can alleviate pathological cardiac remodeling in HF caused by pressure overload.

3.7 TRPV1 Overexpression Protects Mice From TAC-Induced HF by Inhibiting Cardiac Mitochondrial Autophagy

Using the TAC mouse model, we examined how *TRPV1* regulates the levels of autophagy-related proteins. Compared with sham surgery, TAC surgery increased the expression level of sequestosome 1 (SQSTM1) in the cytoplasm while drastically lowering the amounts of Parkin and PTEN-induced kinase 1 (PINK1) ($p < 0.05$, Fig. 5A,B). *TRPV1* overexpression decreased the amount of SQSTM1 and restored Parkin expression ($p < 0.0001$), but it had no discernible effect on PINK1 expression (Fig. 5A,B). In the mitochondrial fraction, TAC increased Parkin and PINK1 levels while decreasing SQSTM1 levels ($p < 0.001$, Fig. 5A,C). Overexpression of *TRPV1* decreased the levels of Parkin and PINK1 ($p < 0.001$, Fig. 5A,C). Autophagy is a lysosome-dependent degradation pathway that promotes ferroptosis by degrading iron storage proteins

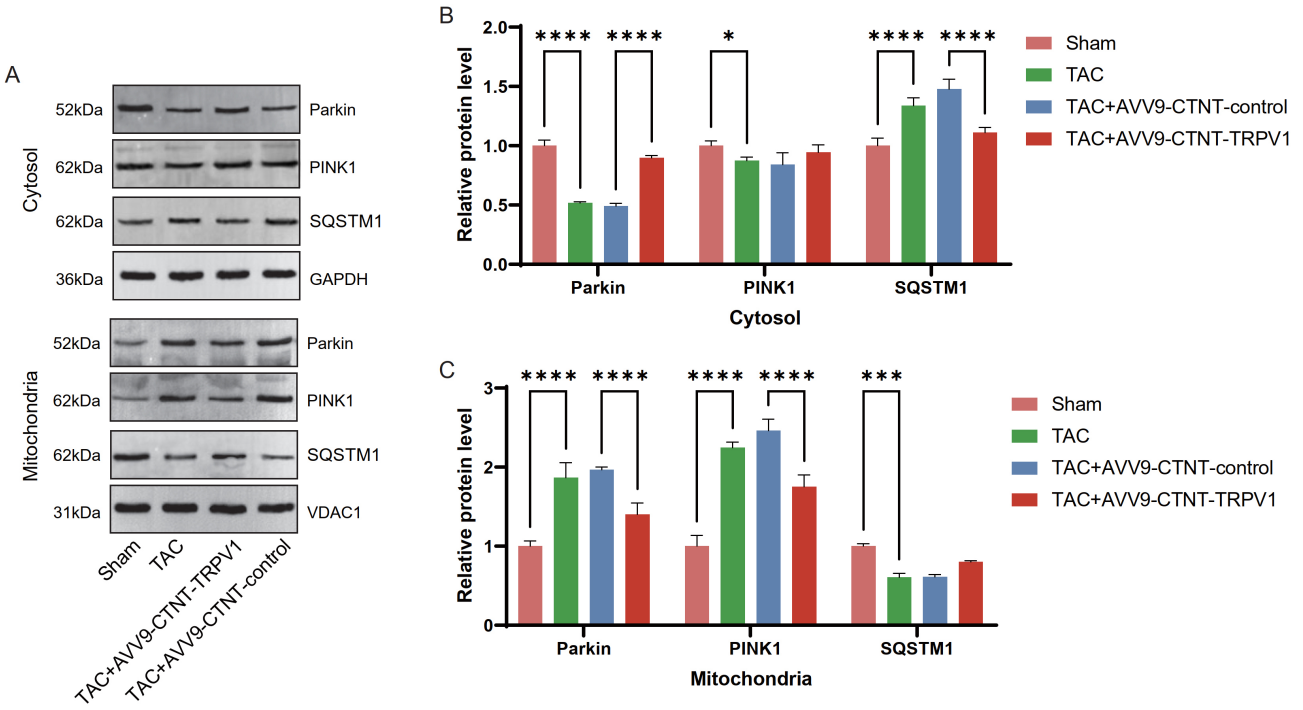

Fig. 5. *TRPV1* overexpression regulates the expression of mitophagy-related proteins in the cytoplasm and mitochondria in the TAC-induced HF model. (A) Representative Western blot images showing the protein expression of mitophagy markers (Parkin, PTEN-induced kinase 1 (PINK1), and sequestosome 1 (SQSTM1)) in the cytoplasm and mitochondria fractions. GAPDH and voltage-dependent anion channel 1 (VDAC1) were used as loading controls for the cytoplasm and mitochondria fractions, respectively. (B) Quantification of the cytoplasmic protein levels of Parkin, PINK1, and SQSTM1 in the experimental groups, with GAPDH as the standard. (C) Quantification of the mitochondrial protein levels of Parkin, PINK1, and SQSTM1 in the experimental groups, with VDAC1 as the standard. n = 8 per group. Data are presented as mean ± standard deviation. *$p < 0.05$, ***$p < 0.001$, ****$p < 0.0001$.

such as ferritin, leading to increased intracellular iron levels and subsequent lipid peroxidation. Therefore, on the basis of the connection between autophagy and ferroptosis, we examined the expression of glutathione peroxidase 4 (GPX4), a ferroptosis marker. Western blot analysis revealed that TAC significantly reduced GPX4 protein levels ($p < 0.0001$, **Supplementary Fig. 8A,B**). Compared with the TAC+AAV9-CTNT-control group, *TRPV1* overexpression significantly upregulated GPX4 expression, indicating that *TRPV1* has a protective effect against TAC-induced ferroptosis ($p < 0.001$, **Supplementary Fig. 8A,B**). These findings suggest that *TRPV1* may respond to TAC-induced cardiac stress by regulating autophagy and ferroptosis pathways.

3.8 TRPV1 Regulates Ferroptosis Through an SFXN2-Dependent Pathway

Previously, we analyzed and verified that *TRPV1* and *SFXN2* interact in HF, but the specific mechanism was unclear. Therefore, we continued to analyze this phenomenon through *in vitro* experiments. To analyze the role of *SFXN2*, we designed three siRNAs targeting *SFXN2*. The qRT–PCR results demonstrated that all three siRNAs effectively reduced *SFXN2* expression in cells, with Si-*SFXN2*#3 (referred to as Si-*SFXN2*) exhibiting the highest knockdown efficacy ($p < 0.0001$, **Supplementary Fig. 9A**). Western blot analysis further confirmed that Si-*SFXN2* significantly decreased *SFXN2* protein levels ($p < 0.01$, **Supplementary Fig. 9B,C**). First, qRT–PCR experiments revealed that, compared with OE-NC, *TRPV1* overexpression significantly increased *SFXN2* mRNA levels, but when TRPV1 was combined with Si-*SFXN2*, its mRNA level was reduced ($p < 0.0001$, Fig. 6A). These results were also confirmed at the protein level, and *SFXN2* knockdown effectively reversed *TRPV1*-induced SFXN2 upregulation ($p < 0.0001$, Fig. 6B,C). Next, we assessed ferroptosis-related markers. The results revealed that *TRPV1* overexpression significantly increased GPX4 protein levels, whereas *SFXN2* knockdown partially reversed this effect ($p < 0.05$, Fig. 6D,E). Consistent with these findings, *TRPV1* overexpression significantly reduced the MDA and Fe^{2+} levels while increasing the GSH content and SOD activity ($p < 0.0001$, Fig. 6F,I). Importantly, these effects were partially reversed after *SFXN2* knockdown ($p < 0.001$, Fig. 6F–I). Taken together, these results suggest that *TRPV1* regulates ferroptosis through an *SFXN2*-dependent pathway.

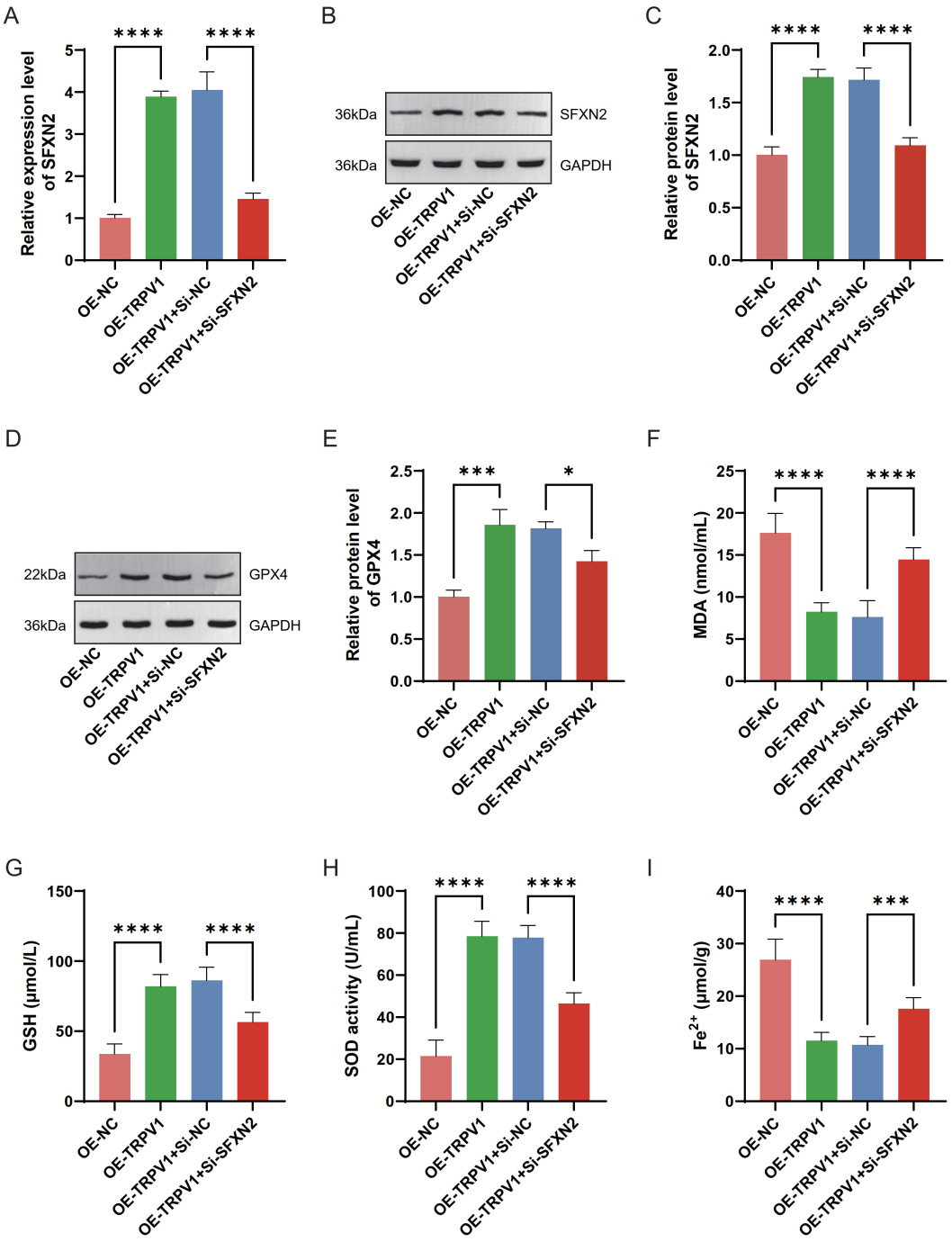

Fig. 6. *TRPV1* regulates ferroptosis in HF through an *SFXN2*-dependent mechanism. (A) qRT–PCR was used to detect the changes in the mRNA level of *SFXN2* after *TRPV1* was overexpressed alone or in combination with down-expressed *SFXN2* in Ang II-induced AC16 cardiomyocytes. (B,C) Western blot was used to detect the protein level of SFXN2 after *TRPV1* was overexpressed alone or in combination with down-expressed *SFXN2* in Ang II-induced AC16 cardiomyocytes. (D,E) Western blot was used to detect the protein level of glutathione peroxidase 4 (GPX4) in Ang II-induced AC16 cardiomyocytes after *TRPV1* was overexpressed alone or in combination with down-expressed *SFXN2*. (F–I) Commercial kits were used to detect the changes in the levels of malondialdehyde (MDA), glutathione (GSH), superoxide dismutase (SOD), and ferrous iron (Fe^{2+}) after *TRPV1* was overexpressed alone or in combination with down-expressed *SFXN2* in Ang II-induced AC16 cardiomyocytes. Each experiment was independently repeated three times. Data are presented as mean ± standard deviation. *$p < 0.05$, ***$p < 0.001$, ****$p < 0.0001$. Si-NC, small interfering RNA negative control; Si-SFXN2, small interfering RNA targeting SFXN2.

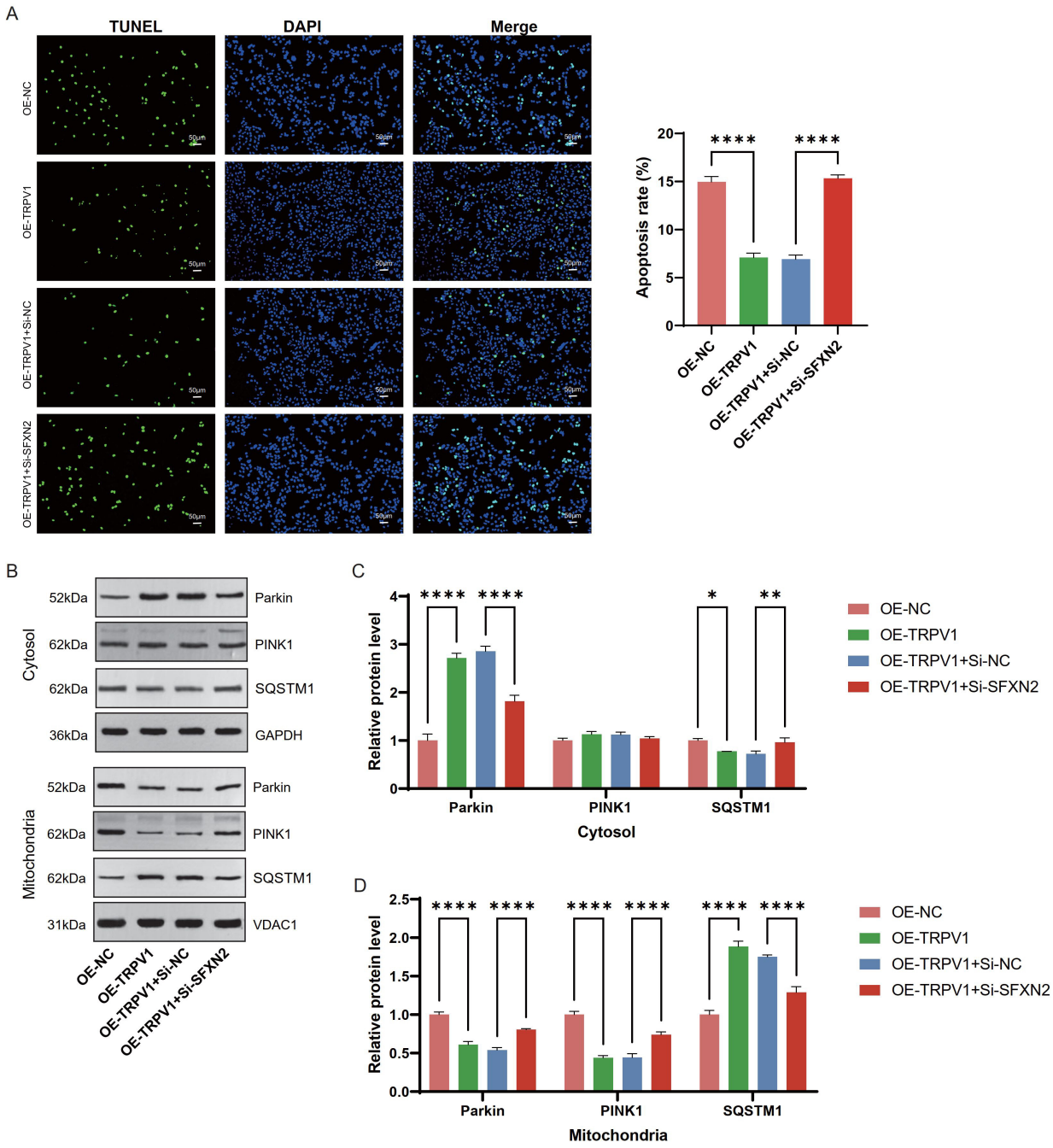

Fig. 7. *TRPV1* inhibits mitochondrial autophagy by regulating PINK1-Parkin-SQSTM1 through upregulating *SFXN2*. (A) In Ang II-induced AC16 cardiomyocytes, terminal deoxynucleotidyl transferase dUTP nick-end labeling (TUNEL) staining was used to detect the apoptosis levels in different experimental groups (OE-NC; OE-*TRPV1*; OE-*TRPV1*+small interfering RNA negative control (Si-NC); OE-*TRPV1*+small interfering RNA targeting *SFXN2* (Si-*SFXN2*)). Left: Representative fluorescence images showing TUNEL-positive cells (green) and nuclear 4′,6-Diamidino-2′-phenylindole (DAPI) staining (blue). Right: Quantification of apoptosis rates among experimental groups. Magnification: 100×. Scale bar = 50 μm. (B) Western blot images showing the protein levels of Parkin, PINK1, and SQSTM1 in the cytoplasmic and mitochondrial fractions. GAPDH and VDAC1 were used as loading controls for the cytoplasmic and mitochondrial fractions, respectively. (C) Quantification of cytoplasmic protein levels with GAPDH as the standard. (D) Quantification of mitochondrial protein levels with VDAC1 as the standard. Each experiment was independently repeated three times. Data are presented as mean ± standard deviation. *$p < 0.05$, **$p < 0.01$, ****$p < 0.0001$.

3.9 TRPV1 Inhibits Mitochondrial Autophagy by Regulating PINK1-Parkin-SQSTM1 Through the Upregulation of SFXN2

Next, we further analyzed the mechanism of action of *SFXN2* and *TRPV1* in an HF model. TUNEL staining demonstrated that *TRPV1* expression alone resulted in a substantial decrease in apoptosis compared with that in the OE-NC group ($p < 0.0001$, Fig. 7A). When SFXN2 knockdown reversed the inhibitory effect of TRPV1 overexpression on cell apoptosis ($p < 0.0001$, Fig. 7A). Subsequent Western blot experiments were used to measure the levels of autophagy-related proteins in the cytoplasm and mitochondria after the transfection of *TRPV1*-overexpressing and *SFXN2*-knockdown vectors. Compared with those in the OE-NC group, *TRPV1* overexpression significantly increased Parkin levels in the cytoplasm while reducing SQSTM1 levels ($p < 0.05$, Fig. 7B,C). *SFXN2* knockdown reversed these *TRPV1*-mediated effects, specifically reducing cytoplasmic Parkin and increasing SQSTM1 levels ($p < 0.01$, Fig. 7B,C). In mitochondria, *TRPV1* overexpression resulted in a substantial reduction in the protein expression of Parkin and PINK1 but increased SQSTM1 expression compared with that in the OE-NC group ($p < 0.0001$, Fig. 7B,D). Conversely, *SFXN2* knockdown significantly reversed these changes, resulting in increased mitochondrial accumulation of Parkin and PINK1, while decreasing SQSTM1 levels ($p < 0.0001$, Fig. 7B,D).

4. Discussion

HF is a severe symptom or advanced stage of certain cardiac disorders. HF can manifest as a decline in cardiac pumping function, decreased ejection function, dyspnea, fatigue, edema and other symptoms. Major advancements have been made in the treatment of HF in recent years, including sodium-dependent glucose transporter 2 (SGLT2) inhibitors for reducing cardiac workload and increasing cardiac metabolism, glucagon like peptide 1 (GLP-1) receptor agonists/SGLT2 inhibitors as first-line treatments for HF patients with reduced ejection fraction (HFrEF), and β-blockers for normalizing cardiac function [18,19]. Moreover, increasing cardiac function, promoting myocardial regeneration and normalizing energy metabolism through specific gene delivery is an emerging treatment method [20]. In this study, through bioinformatic analysis and experimental validation, we identified *SFXN2* as a key downstream target of *TRPV1* and described a novel cardioprotective mechanism involving the regulation of *SFXN2*-dependent ferroptosis and mitochondrial autophagy by TRPV1. Specifically, we found that *TRPV1* expression was downregulated in both Ang II-treated cardiomyocytes and TAC-induced HF models. Importantly, upregulating *TRPV1* expression normalized cardiac function and attenuated pathological remodeling. These findings elucidate a novel mechanism by which *TRPV1* exerts cardioprotective effects and suggest a potential therapeutic strategy for treating HF by targeting *TRPV1-SFXN2* signaling.

Research has shown that changes in myocardial calcium ions regulate the process of contraction and blood flow in HF. In the context of HF, the interaction between myocardial cells and the calcium ion regulatory mechanism in the body is impaired, resulting in unstable contraction and expansion of the heart [21]. This change, in turn, affects the blood transfusion capacity of the heart and thus causes HF in patients. To explore the regulatory mechanism involved in this process, we investigated the role of *TRPV1* under pathological conditions induced by Ang II. Our results indicated that Ang II therapy significantly reduced *TRPV1* expression in AC16 cardiomyocytes. Fluorescence analysis indicated that *TRPV1* overexpression dramatically decreased the intracellular Ca^{2+} level in AC16 cardiomyocytes, indicating that TRPV1 is essential for preserving calcium homeostasis.

Oxidative stress contributes to the progression of HF through many pathways, which can cause myocardial cell damage and mitochondrial dysfunction and induce inflammatory responses by activating the nuclear factor kappa-light-chain-enhancer of activated B cells (NF-κB) signaling pathway [22]. Increased ROS has been shown to lead to protein and DNA damage, promote cell apoptosis and necrosis, and ultimately lead to cardiac dysfunction [23]. Given the established relationship between calcium homeostasis and oxidative stress in cardiac pathophysiology, the current investigation investigated the effects of *TRPV1* on oxidative stress markers. The results revealed that *TRPV1* overexpression protected cardiomyocytes against Ang II-induced death. Importantly, *TRPV1* significantly attenuated Ang II-induced oxidative stress, as manifested by reduced ROS levels. These findings indicate that *TRPV1* may protect against HF progression by lowering oxidative stress, offering insights into potential therapeutic targets for HF.

Through sequencing data, we screened 195 upregulated and 54 downregulated *TRPV1*-related DEGs from AC16 cardiomyocytes with *TRPV1* overexpression. According to the enrichment analysis, these genes were connected to pathways such as the apelin signaling pathway, herpes simplex virus 1 infection, alcoholism, the IL-17 signaling pathway, influenza A, the chemokine signaling pathway, and the NOD-like receptor signaling pathway. Through a variety of signaling pathways, *TRPV1* may be crucial to the onset and progression of HF, according to the roles of these enriched pathways. The apelin signaling pathway is one such pathway and has been extensively recognized to be linked to HF [24]. Apelin binds to the apelin receptor (APJ), regulates cardiac function and vasodilation, and has a crucial protective effect [25]. The pathological process of HF is often accompanied by an inflammatory response, and chemokines such as C-C motif chemokine ligand 2 (CCL2) and C-X-C motif chemokine ligand 12

(CXCL12) play key roles in myocardial injury, fibrosis and remodeling [26,27]. Influenza virus infection can also induce viral myocarditis, which can lead to HF in severe cases [28]. NOD-like receptor family pyrin domain containing 3 (NLRP3) inflammasomes in NOD-like receptors (NLRs) promote myocardial fibrosis and ventricular remodeling by releasing interleukin-18 (IL-18) and interleukin-1 beta (IL-1β) [29]. IL-17 triggers the production of inflammatory molecules, including tumor necrosis factor-alpha (TNF-α) and interleukin-6 (IL-6), which can worsen HF [30].

Studies have revealed that mitochondrial dysfunction is directly associated with the incidence and progression of HF, with dysfunctional mitochondrial energy metabolism, gene mutations, oxidative stress damage, and calcium homeostasis imbalance being major variables that cause HF [31,32]. In-depth studies into the association between mitochondrial malfunction and HF may lead to the discovery of novel therapeutic targets. In this study, seven genes related to *TRPV1* (*G0S2*, *SLC25A24*, *SDS*, *SFXN2*, *CKMT2*, *TPPP*, and *LDHAL6B*) were identified from MitoRGs. Research has revealed substantial positive associations between the *TRPV1*, *SFXN2*, and *LDHAL6B* genes. qRT–PCR was used to validate the changes in the expression of these genes in Ang II-treated AC16 cells. Among these genes, *SDS*, *SFXN2*, *CKMT2*, *TPPP*, and *LDHAL6B* were significantly overexpressed after *TRPV1* overexpression. These results suggest that *TRPV1* has a potential connection with mitochondrial regulation. Given that SFXN2 plays a crucial role in controlling iron metabolism and mitochondrial activity and that the relationship between *LDHAL6B* and mitochondria has not been explored in detail, *SFXN2* was selected as a key downstream target of *TRPV1* for further study. SFXN2, an evolutionarily conserved protein found in mitochondria, plays a role in the metabolism of iron within the mitochondria. Our study revealed that *TRPV1* regulates *SFXN2* expression in cardiomyocytes, suggesting a potential link between calcium signaling and mitochondrial iron metabolism in HF.

The TAC model is a common experimental model of left ventricular hypertrophy (LVH) and HF and has been widely used to study the processes of compensatory or maladaptive cardiac remodeling, cardiac hypertrophy, fibrosis, and dysfunction [33,34]. To evaluate the therapeutic potential of TRPV1 in HF induced by pressure overload, we used this well-established model in our study. The increased ejection fraction and fractional shortening in the TAC-induced HF model demonstrated normalized cardiac function in this study due to *TRPV1* overexpression. *TRPV1* overexpression reduced the TAC-induced increase in cardiac stress indicators (ANP and β-MHC) and restored SFXN2 protein levels, as determined by Western blot analysis. These cardiac stress markers play important roles in HF. Among them, ANP, as a protective molecule, attempts to alleviate HF symptoms by reducing blood pressure and reducing cardiac workload [35]. The upregulation of β-MHC reflects reduced myocardial contractility and cardiac remodeling, which are key factors in HF progression [36]. Furthermore, *TRPV1* overexpression regulated autophagy-related proteins and reversed TAC-induced changes in Parkin, PINK1, and SQSTM1. This regulation of autophagy and ferroptosis pathways, particularly through increased GPX4 expression, suggests that *TRPV1* prevents TAC-induced HF by alleviating mitochondrial dysfunction and ferroptosis.

Excessive ROS generation during HF development is caused by mitochondrial dysfunction and is a major factor in the promotion of oxidative damage and disruption of cellular homeostasis [37]. When mitochondrial function is impaired, cardiomyocytes are unable to effectively clear damaged mitochondria, resulting in ROS accumulation and subsequent cell death. Recent studies have shown that intracellular stress caused by lipid peroxidation, oxidative stress, and inflammatory responses triggers autophagy in endothelial cells and cardiomyocytes, particularly by affecting cardiac iron metabolism [38,39]. This dysregulation of iron homeostasis may lead to ferroptosis, a newly recognized form of regulated cell death. In HF with preserved ejection fraction (HFpEF), the inhibition of ferroptosis has been shown to alleviate pathological cardiac remodeling, including cardiac fibrosis and decreased capillary density [40]. Notably, targeting the *ACSL4*-ferroptosis-ferroptosis signaling axis may represent a promising therapeutic strategy for HF [41]. For example, phosphoglycerate mutase family member 5 (*PGAM5*) has a protective effect against ferroptosis through a reduction in oxidative stress mediated by the kelch-like ECH-associated protein 1 (KEAP1)/nuclear factor erythroid 2-related factor 2 (NRF2) pathway [42]. Moreover, GPX4, a key antiferroptosis protein, can be regulated through the autophagy–lysosomal pathway, in which excessive autophagy may lead to *GPX4* degradation and subsequent ferroptosis [43]. Therefore, understanding the role of ferroptosis in HF may help develop new targeted therapies.

Recent studies have proposed a complex relationship between mitophagy and ferroptosis in HF. The PINK1-Parkin-SQSTM1 pathway has been shown to regulate mitochondrial quality control through selective mitophagy [44]. PINK1 phosphorylation recruits Parkin to depolarized mitochondria, thereby activating SQSTM1-mediated clearance. Notably, this mechanism has been implicated in ferroptosis, as autophagy can promote ferroptosis by disrupting iron storage proteins, leading to increased intracellular iron accumulation and lipid peroxidation [45]. This connection is further supported by another study showing that under conditions of oxidative stress, such as hypoxia/reoxygenation injury, disturbances in iron metabolism and GSH homeostasis promote ferroptosis through alterations in GPX4 and iron transport-related proteins [46]. Similar regulatory mechanisms have been observed for other molecules, such as nucleolar protein

family member 4 (*NPLOC4*), which promotes mitochondrial function through endoplasmic reticulum oxidoreductase 1 alpha (ERO1α) expression and mitophagy mediated by the β-catenin/glycogen synthase kinase 3 beta (GSK3β) pathway [47]. In this study, we demonstrated that *TRPV1* regulates ferroptosis through an *SFXN2*-dependent pathway. Overexpression of *TRPV1* increased the amount of *SFXN2* mRNA and protein, which in turn increased GPX4 expression and decreased the levels of MDA, Fe^{2+}, and oxidative stress markers. These effects were largely reversed by *SFXN2* knockdown, demonstrating the key role of *SFXN2* in *TRPV1*-mediated control of ferroptosis. In addition, we found that *TRPV1* inhibited mitophagy by regulating the PINK1-Parkin-SQSTM1 pathway. These effects were reversed after *SFXN2* knockdown, indicating that *TRPV1* may prevent HF by coordinating *SFXN2*-dependent ferroptosis and mitophagy pathways.

5. Conclusion

Our findings revealed that *TRPV1* expression was downregulated in Ang II-treated cardiomyocytes and the TAC-induced HF model, whereas the upregulation of *TRPV1* expression significantly normalized cardiac function and alleviated pathological remodeling. Mechanistically, *TRPV1* upregulated *SFXN2* expression, increased GPX4 levels and antioxidant capacity, and regulated PINK1-Parkin-SQSTM1 distribution in the cytoplasm and mitochondria. Taken together, these findings identify *TRPV1* as a novel cardioprotective factor through *SFXN2*-dependent ferroptosis regulation and mitophagy in HF.

Availability of Data and Materials

All data are available upon the reasonable request to the corresponding authors.

Author Contributions

PL: methodology, writing, review and editing, and approval for final version. LYL and RHL: investigation, data curation, formal analysis, and approval for final version. MMF, JJK and BG: investigation, data curation, software, and approval for final version. SGW: methodology, writing, review and editing. JW: conceptualization, review and editing. RX: methodology, review and approval for final version. All authors contributed to the article and approved the submitted version. All authors contributed to editorial changes in the manuscript. All authors have participated sufficiently in the work and agreed to be accountable for all aspects of the work.

Ethics Approval and Consent to Participate

The study was authorized by the Anhui University of Chinese Medicine First Affiliated Hospital Animal Ethics Committee's Institutional Animal Care and Use Committee (AZYFY-2024-1006). All experiments were conducted in accordance with the 3R principles.

Acknowledgment

We would like to thank the platform support provided by Anhui Provincial Key Laboratory of Meridians and Organs.

Funding

The present research was funded by the National Key R&D Program of China (2022YFC3500502) and Anhui Provincial Scientific Research Planning Project (2023AH050796).

Conflict of Interest

The authors declare no conflict of interest.

Supplementary Material

Supplementary material associated with this article can be found, in the online version, at https://doi.org/10.31083/FBL37052.

References

[1] Dini FL, Pugliese NR, Ameri P, Attanasio U, Badagliacca R, Correale M, *et al*. Right ventricular failure in left heart disease: from pathophysiology to clinical manifestations and prognosis. Heart Failure Reviews. 2023; 28: 757–766. https://doi.org/10.1007/s10741-022-10282-2.

[2] Jering K, Claggett B, Redfield MM, Shah SJ, Anand IS, Martinez F, *et al*. Burden of Heart Failure Signs and Symptoms, Prognosis, and Response to Therapy: The PARAGON-HF Trial. JACC. Heart Failure. 2021; 9: 386–397. https://doi.org/10.1016/j.jchf.2021.01.011.

[3] Wang A, Guo Y, Ding S, Yu Y, Yuan Z, Zhang H, *et al*. The Investigation of the Molecular Mechanism of Morinda officinalis How in the Treatment of Heart Failure. Frontiers in Bioscience (Landmark Edition). 2023; 28: 34. https://doi.org/10.31083/j.fbl2802034.

[4] Deshmukh K, Khanna A. Implications of Managing Chronic Obstructive Pulmonary Disease in Cardiovascular Diseases. Tuberculosis and Respiratory Diseases. 2021; 84: 35–45. https://doi.org/10.4046/trd.2020.0088.

[5] Bernad BC, Tomescu MC, Velimirovici DE, Andor M, Lungeanu D, Enătescu V, *et al*. Impact of Stress and Anxiety on Cardiovascular Health in Pregnancy: A Scoping Review. Journal of Clinical Medicine. 2025; 14: 909. https://doi.org/10.3390/jcm14030909.

[6] Ahmad H, Khan H, Haque S, Ahmad S, Srivastava N, Khan A. Angiotensin-Converting Enzyme and Hypertension: A Systemic Analysis of Various ACE Inhibitors, Their Side Effects, and Bioactive Peptides as a Putative Therapy for Hypertension. Journal of the Renin-angiotensin-aldosterone System: JRAAS. 2023; 2023: 7890188. https://doi.org/10.1155/2023/7890188.

[7] Khan O, Patel M, Tomdio AN, Beall J, Jovin IS. Beta-Blockers in the Prevention and Treatment of Ischemic Heart Disease: Evidence and Clinical Practice. Heart Views: the Official Journal of the Gulf Heart Association. 2023; 24: 41–49. https://doi.org/10.4103/heartviews.heartviews_75_22.

[8] Peng F, Liao M, Jin W, Liu W, Li Z, Fan Z, *et al*. 2-APQC, a small-molecule activator of Sirtuin-3 (SIRT3), alleviates myocardial hypertrophy and fibrosis by regulating mitochondrial homeostasis. Signal Transduction and Targeted Therapy. 2024; 9: 133. https://doi.org/10.1038/s41392-024-01816-1.

[9] Yan Q, Tang J, Zhang X, Wu L, Xu Y, Wang L. Does Tran-

sient Receptor Potential Vanilloid Type 1 Alleviate or Aggravate Pathological Myocardial Hypertrophy? Frontiers in Pharmacology. 2021; 12: 681286. https://doi.org/10.3389/fphar.2021.681286.

[10] Horton JS, Buckley CL, Stokes AJ. Successful TRPV1 antagonist treatment for cardiac hypertrophy and heart failure in mice. Channels (Austin, Tex.). 2013; 7: 17–22. https://doi.org/10.4161/chan.23006.

[11] Zhu L, Gao B, Gong TT, Liu P, Li L, Xia R, *et al*. Effect of moxibustion at "Xinshu" (BL15) and "Feishu" (BL13) on expression of TRPV1 and CGRP in the myocardial tissue of chronic heart failure rats. Zhen Ci Yan Jiu = Acupuncture Research. 2024; 49: 551–557. https://doi.org/10.13702/j.1000-0607.20230820.

[12] Fang X, Ardehali H, Min J, Wang F. The molecular and metabolic landscape of iron and ferroptosis in cardiovascular disease. Nature Reviews. Cardiology. 2023; 20: 7–23. https://doi.org/10.1038/s41569-022-00735-4.

[13] Chen Y, Li X, Wang S, Miao R, Zhong J. Targeting Iron Metabolism and Ferroptosis as Novel Therapeutic Approaches in Cardiovascular Diseases. Nutrients. 2023; 15: 591. https://doi.org/10.3390/nu15030591.

[14] Morales PE, Arias-Durán C, Ávalos-Guajardo Y, Aedo G, Verdejo HE, Parra V, *et al*. Emerging role of mitophagy in cardiovascular physiology and pathology. Molecular Aspects of Medicine. 2020; 71: 100822. https://doi.org/10.1016/j.mam.2019.09.006.

[15] Chen Y, Qian J, Ding P, Wang W, Li X, Tang X, *et al*. Elevated SFXN2 limits mitochondrial autophagy and increases iron-mediated energy production to promote multiple myeloma cell proliferation. Cell Death & Disease. 2022; 13: 822. https://doi.org/10.1038/s41419-022-05272-z.

[16] Bhullar SK, Dhalla NS. Angiotensin II-Induced Signal Transduction Mechanisms for Cardiac Hypertrophy. Cells. 2022; 11: 3336. https://doi.org/10.3390/cells11213336.

[17] Zhang F, Zeng Z, Zhang J, Li X, Yang W, Wei Y, *et al*. Pterostilbene attenuates heart failure by inhibiting myocardial ferroptosis through SIRT1/GSK-3β/GPX4 signaling pathway. Heliyon. 2024; 10: e24562. https://doi.org/10.1016/j.heliyon.2024.e24562.

[18] Koniari I, Velissaris D, Kounis NG, Koufou E, Artopoulou E, de Gregorio C, *et al*. Anti-Diabetic Therapy, Heart Failure and Oxidative Stress: An Update. Journal of Clinical Medicine. 2022; 11: 4660. https://doi.org/10.3390/jcm11164660.

[19] Cosentino F, Bhatt DL, Marx N, Verma S. The year in cardiovascular medicine 2021: diabetes and metabolic disorders. European Heart Journal. 2022; 43: 263–270. https://doi.org/10.1093/eurheartj/ehab876.

[20] Sapna F, Raveena F, Chandio M, Bai K, Sayyar M, Varrassi G, *et al*. Advancements in Heart Failure Management: A Comprehensive Narrative Review of Emerging Therapies. Cureus. 2023; 15: e46486. https://doi.org/10.7759/cureus.46486.

[21] Procaccini DE, Sawyer JE, Watt KM. Pharmacology of Cardiovascular drugs. Critical Heart Disease in Infants and Children (pp.192–212. e196). Elsevier: Amsterdam, Netherlands. 2019. https://doi.org/10.1016/B978-1-4557-0760-7.00019-X.

[22] Peng ML, Fu Y, Wu CW, Zhang Y, Ren H, Zhou SS. Signaling Pathways Related to Oxidative Stress in Diabetic Cardiomyopathy. Frontiers in Endocrinology. 2022; 13: 907757. https://doi.org/10.3389/fendo.2022.907757.

[23] Nikfarjam S, Singh KK. DNA damage response signaling: A common link between cancer and cardiovascular diseases. Cancer Medicine. 2023; 12: 4380–4404. https://doi.org/10.1002/cam4.5274.

[24] de Oliveira AA, Vergara A, Wang X, Vederas JC, Oudit GY. Apelin pathway in cardiovascular, kidney, and metabolic diseases: Therapeutic role of apelin analogs and apelin receptor agonists. Peptides. 2022; 147: 170697. https://doi.org/10.1016/j.peptides.2021.170697.

[25] Alotibi BHF, Al-Hazmi AF, Imam KZ, AlMalkei WR. Pharmacological agonists of the Apelin (APJ) Receptor, reviewing mechanism of action. Journal of International Crisis and Risk Communication Research. 2024; 7: 659–663. https://doi.org/10.63278/jicrcr.vi.794.

[26] Chen B, Frangogiannis NG. Chemokines in Myocardial Infarction. Journal of Cardiovascular Translational Research. 2021; 14: 35–52. https://doi.org/10.1007/s12265-020-10006-7.

[27] Hedayati-Moghadam M, Hosseinian S, Paseban M, Shabgah AG, Gholizadeh J, Jamialahmadi T, *et al*. The Role of Chemokines in Cardiovascular Diseases and the Therapeutic Effect of Curcumin on CXCL8 and CCL2 as Pathological Chemokines in Atherosclerosis. Advances in Experimental Medicine and Biology. 2021; 1328: 155–170. https://doi.org/10.1007/978-3-030-73234-9_11.

[28] Martens CR, Accornero F. Viruses in the Heart: Direct and Indirect Routes to Myocarditis and Heart Failure. Viruses. 2021; 13: 1924. https://doi.org/10.3390/v13101924.

[29] Shen S, Wang Z, Sun H, Ma L. Role of NLRP3 Inflammasome in Myocardial Ischemia-Reperfusion Injury and Ventricular Remodeling. Medical Science Monitor: International Medical Journal of Experimental and Clinical Research. 2022; 28: e934255. https://doi.org/10.12659/MSM.934255.

[30] Szabo TM, Frigy A, Nagy EE. Targeting Mediators of Inflammation in Heart Failure: A Short Synthesis of Experimental and Clinical Results. International Journal of Molecular Sciences. 2021; 22: 13053. https://doi.org/10.3390/ijms222313053.

[31] Liu M, Lv J, Pan Z, Wang D, Zhao L, Guo X. Mitochondrial dysfunction in heart failure and its therapeutic implications. Frontiers in Cardiovascular Medicine. 2022; 9: 945142. https://doi.org/10.3389/fcvm.2022.945142.

[32] Zhou B, Tian R. Mitochondrial dysfunction in pathophysiology of heart failure. The Journal of Clinical Investigation. 2018; 128: 3716–3726. https://doi.org/10.1172/JCI120849.

[33] Beslika E, Leite-Moreira A, De Windt LJ, da Costa Martins PA. Large animal models of pressure overload-induced cardiac left ventricular hypertrophy to study remodelling of the human heart with aortic stenosis. Cardiovascular Research. 2024; 120: 461–475. https://doi.org/10.1093/cvr/cvae045.

[34] Eitner F, Richter B, Schwänen S, Szaroszyk M, Vogt I, Grund A, *et al*. Comprehensive Expression Analysis of Cardiac Fibroblast Growth Factor 23 in Health and Pressure-induced Cardiac Hypertrophy. Frontiers in Cell and Developmental Biology. 2022; 9: 791479. https://doi.org/10.3389/fcell.2021.791479.

[35] Ilatovskaya DV, Levchenko V, Winsor K, Blass GR, Spires DR, Sarsenova E, *et al*. Effects of elevation of ANP and its deficiency on cardiorenal function. JCI Insight. 2022; 7: e148682. https://doi.org/10.1172/jci.insight.148682.

[36] Bai L, Zhao Y, Zhao L, Zhang M, Cai Z, Yung KKL, *et al*. Ambient air $PM_{2.5}$ exposure induces heart injury and cardiac hypertrophy in rats through regulation of miR-208a/b, α/β-MHC, and GATA4. Environmental Toxicology and Pharmacology. 2021; 85: 103653. https://doi.org/10.1016/j.etap.2021.103653.

[37] Li A, Gao M, Liu B, Qin Y, Chen L, Liu H, *et al*. Mitochondrial autophagy: molecular mechanisms and implications for cardiovascular disease. Cell Death & Disease. 2022; 13: 444. https://doi.org/10.1038/s41419-022-04906-6.

[38] Shi S, Chen Y, Luo Z, Nie G, Dai Y. Role of oxidative stress and inflammation-related signaling pathways in doxorubicin-induced cardiomyopathy. Cell Communication and Signaling: CCS. 2023; 21: 61. https://doi.org/10.1186/s12964-023-01077-5.

[39] Li JY, Liu SQ, Yao RQ, Tian YP, Yao YM. A Novel Insight Into the Fate of Cardiomyocytes in Ischemia-Reperfusion In-

jury: From Iron Metabolism to Ferroptosis. Frontiers in Cell and Developmental Biology. 2021; 9: 799499. https://doi.org/10.3389/fcell.2021.799499.

[40] Su H, Cantrell AC, Chen JX, Gu W, Zeng H. SIRT3 Deficiency Enhances Ferroptosis and Promotes Cardiac Fibrosis via p53 Acetylation. Cells. 2023; 12: 1428. https://doi.org/10.3390/cells12101428.

[41] Bi X, Wu X, Chen J, Li X, Lin Y, Yu Y, *et al*. Characterization of ferroptosis-triggered pyroptotic signaling in heart failure. Signal Transduction and Targeted Therapy. 2024; 9: 257. https://doi.org/10.1038/s41392-024-01962-6.

[42] Li S, Wen P, Zhang D, Li D, Gao Q, Liu H, *et al*. PGAM5 expression levels in heart failure and protection ROS-induced oxidative stress and ferroptosis by Keap1/Nrf2. Clinical and Experimental Hypertension (New York, N.Y.: 1993). 2023; 45: 2162537. https://doi.org/10.1080/10641963.2022.2162537.

[43] Chen X, Yu C, Kang R, Kroemer G, Tang D. Cellular degradation systems in ferroptosis. Cell Death and Differentiation. 2021; 28: 1135–1148. https://doi.org/10.1038/s41418-020-00728-1.

[44] Iorio R, Celenza G, Petricca S. Mitophagy: Molecular Mechanisms, New Concepts on Parkin Activation and the Emerging Role of AMPK/ULK1 Axis. Cells. 2021; 11: 30. https://doi.org/10.3390/cells11010030.

[45] Zhou J, Li XY, Liu YJ, Feng J, Wu Y, Shen HM, *et al*. Full-coverage regulations of autophagy by ROS: from induction to maturation. Autophagy. 2022; 18: 1240–1255. https://doi.org/10.1080/15548627.2021.1984656.

[46] Pang P, Si W, Wu H, Ju J, Liu K, Wang C, *et al*. YTHDF2 Promotes Cardiac Ferroptosis *via* Degradation of SLC7A11 in Cardiac Ischemia-Reperfusion Injury. Antioxidants & Redox Signaling. 2024; 40: 889–905. https://doi.org/10.1089/ars.2023.0291.

[47] Ren K, Luan Y, Sun Y, Huang S, Zhang S, Yang Y, *et al*. NPLOC4 aggravates heart failure by regulating ROS and mitochondrial function. International Immunopharmacology. 2024; 142: 113199. https://doi.org/10.1016/j.intimp.2024.113199.